INDIAN JOURNAL OF SCIENCE AND TECHNOLOGY

*Corresponding author.

msrphd2022@gmail.com

Tailoring the Inherent Magnetism of N:CdS Nanoparticles with Co²⁺ Doping

M Surya Sekhar Reddy[1,2]*, **C Sai Vandana**[3], **Y B Kishore Kumar**[4]

1 Department of Physics, JNTUA, Ananthapuramu, A.P, India
2 Department of Physics, SVCR Government Degree College, Palamaner, A.P, India
3 Department of Physics, Government Degree College for Women, Srikalahasti, A.P., India
4 Department of Physics, Sree Vidyanikethan Engineering College, Tirupathi, A.P, India

Abstract

Objectives: The purpose of this study is to report the changes in structural, electrical, optical, and magnetic properties of N: CdS nanoparticles with Co²⁺ doping, which have applications in the fields of opto-magnetic and spintronic devices. **Methods:** Nitrogen and cobalt-co-doped CdS nanoparticles (NPs) have been prepared using the surfactant-assisted chemical co-precipitate method. **Findings:** The X-Ray Diffraction (XRD) studies with X'pert High Score Plus software confirm the existence of multiphase and the size of the as prepared particles in the nanorange (1-2 nm). UV-VIS. absorption spectral analysis showed a considerable blue shift with the inclusion of nitrogen and a further Burstein-mass effect, i.e., a red shift with increasing Co²⁺ ion concentration. The strong green light emissions observed in photoluminescence (PL) studies are attributed to the trapping of Co²⁺ and N³⁻ ions in F-centers. The characteristic $g = 1.995$ obtained from electron paramagnetic resonance (EPR) studies confirms the inclusion of nitrogen in the tetrahedral sites of the CdS core and the increased stability of nanoparticles. The vibrating sample magnetometer (VSM) studies revealed novel magnetic behaviour of nanoparticles at low fields. **Novelty:** Tunable band gap variations, ferromagnetic nature at low fields are the unique features observed in NPs with useful applications in the fields of opto-magnetic and spintronic applications. Nitrogen and cobalt-co-doped CdS nanoparticles (NPs) have been prepared using the surfactant assisted chemical co-precipitate method. The X-ray diffraction (XRD) studies with X'pert high score plus software confirm the existence of multiple phases and the size of the as prepared particles in the nanorange (1-2nm). UV-VIS absorption spectral analysis showed a considerable blue shift with the inclusion of nitrogen and a further Burstein-mass effect, i.e., a red shift with increasing Co²⁺ ion concentration. The strong green light emission observed in photoluminescence (PL) studies is attributed to the trapping of Co²⁺, N³⁻ ions in F-centers. The characteristic $g = 1.995$ obtained from electron paramagnetic resonance (EPR) studies confirms the inclusion of nitrogen in the tetrahedral sites of the CdS core and the increased stability of nanoparticles. The vibrating sample magnetometer (VSM) studies revealed novel magnetic behaviour of nanoparticles at low fields.

Tunable band gap variations, ferromagnetic nature at low fields are the unique features observed in NPs with useful applications in the fields of opto-magnetic and spintronic applications.

Keywords: Cds; Cobalt; Nitrogen; UV-Vis; EPR; VSM

1 Introduction

In II-VI semiconductor compounds, CdS is a wide band gap semiconductor useful in heterojunction solar cells, light-emitting diodes, address decoders, biological sensors, photocatalytic devices, and gas detectors[1]. The band gap is easily tunable by replacing a small number of cation impurities as well as anion impurities[2]. A large number of studies are available on the injection of cation impurities to produce modifications in optical, electrical, magnetic, and structural properties. The transition elements doped with CdS have the advantage of producing magnetic materials known as diluted magnetic semiconductors (DMS), which play an important role in spintronic applications where spin and charge transportation are needed to control the properties of devices. In addition to magnetic properties, optical, electrical, and structural properties have created greater interest in modern research to produce next-generation smart devices[3]. Many reports are available on Cr, Co, Mn, Ni, Fe, Zn, and Cu used as dopants as well as co-dopants in CdS nanoparticles with different synthesis methods[3–7].

Among all the transition metals, due to the smaller ionic radius (79 pm), Co^{2+} easily substitutes Cd^{2+} (ionic radius 109 pm) in the lattice of cadmium sulfide. Many researchers prepared and studied Co^{2+} doped and co-doped with other transitional elements in CdS[1,5]. Giribabu et al., prepared Co^{2+} as a dopant and co-dopant in CdS nanoparticles and reported structural, optical, and magnetic properties[8]. Recent studies have revealed that the stability of nanoparticles is a major problem. In order to improve stability and fluorescence properties, O, Se, Te, and N are essential substitutional elements[9–13]. The stability of the compound is improved by doping elements that are capable of forming secondary compounds. Due to its high electronegativity and ability to exist in different ionic states (N^{3-} with a radius of 132 pm, N^{3+} with a radius of 30 pm, and N^{5+} with a radius of 27 pm), nitrogen may form secondary compounds when it is included in II-VI semiconductor (CdS) nanoparticles.

The possibility of different ionic states for N acts as an anionic substitution as well as the cationic substitution in II-VI compounds, particularly in CdS, when compared with chalcogens and halogens. Cationic substitution studies in CdS are available[10], but no anionic substitution studies are available in CdS nanoparticles. Recently, Popov et al., doped nitrogen in ZnS[14] and Shi et al., reported an improvement in the stability of CdS nanostructures by the inclusion of nitrogen[12].

Different methods are available to prepare nanoparticles, among them, the simple chemical co-precipitation method is one of the best methods due to the low requirement of material quantities, large mass production, and best control over the particle size by means of capping agents. The inclusion of nitrogen requires a high temperature and a controlled environment. In the present study, we have successfully prepared nitrogen co-doped with cobalt in CdS at room temperature using the co-precipitation method. 2-Mercaptoethanol is used as a capping agent and has reported considerable changes in the structural, mechanical, electrical, optical, and magnetic properties of CdS NPs. Tunable band gap variations and ferromagnetic nature at low fields are the unique features noticed in synthesized NPs with applications in the fields of opto-magnetic and spintronic applications.

2 Methodology

Sigma Aldrich AR grade 99.9% purity chemicals were used to prepare CdS and $Cd_{1-x}Co_xN_{0.06}S_{0.94}$(where (where x = 0, 0.02, 0.04, 0.06, and 0.08) nanoparticles using the chemical co-precipitation method. For the anionic precursors, sodium sulfide (for sulfur), thiourea (for nitrogen) were used, and for the cationic precursors, cadmium acetate dihydrate (for cadmium) and cobalt acetate tetrahydrate (for cobalt) were used. 0.2M solutions of precursors were prepared separately using deionized water as per the stoichiometric ratio and stirred for 30 minutes. The cationic precursor cadmium acetate is taken in a conical flask placed on a magnetic stirrer, and cobalt acetate tetra hydrate and 0.5 ml of 2-mercaptoethanol (capping agent) are added dropwise simultaneously under constant stirring for 30 minutes, The anionic precursors thiourea and sodium sulfide were then added dropwise and stirred for 7 h. Precipitates were filtered and washed several times using deionized water to remove any impurities. Kept the precipitates in a watch glass to dry naturally for 24h in the laboratory and ground them into a fine powder.

Structural analysis was carried out with a Bruker D8 advance, Germany, X-ray diffractometer with a Cu K_α radiation wavelength of 1.540Å. Carl FESEM03-81 was used to study morphology. The Oxford EDAX with Carl FESEM was used to estimate the chemical composition. Perkins- Elmer LAMDA950 UV-VIS-NIR spectrometer was used to record the diffuse reflectance as well as absorption spectra ranging from 200 nm to 2400nm. The JES200 CW ESR spectrometer was used to record the spectra with x-band microwave excitation at a microwave frequency of 9.5 GHz to study the electronic states. Room-temperature photoluminescence (PL) spectra were recorded using the JY Fluorolog-3-11 spectrometer. The Lakeshore VSM 7407 was used to record the magnetic field versus intensity of magnetization at room temperature.

3 Results and Discussion

3.1. Structural studies

The Rietveld refinement XRD patterns of CdS, $Cd_{1-x}Co_xN_{0.06}S_{0.94}$ (where x = 0, 0.02, 0.04, 0.06, and 0.08) nanoparticles are shown in Figure 1. The blue and red plots represent the calculated and observed values, respectively. Three broad peaks are observed at (110), (111) of Co_3N_2, and (110) of CdS. All these peaks perfectly match the cubic zinc blend (JCPDS 10-454) phase for pure CdS, and along with the above hexagonal wurtzite (JCPDS card No. 41-1049) phase at lower doping concentrations (x = 0, 0.02, and 0.04), the mixed phases are an indication of peak broadening. The low intensity peaks at an angle of 43.7° observed for (x = 0.06, 0.08%) perfectly match the Co_3N_2 phase [indicated in (111) Miller- indices]. This indicates the inclusion of nitrogen and cobalt into the CdS to form a solid solution. The peak broadening and shifting of principle peaks towards higher 2θ angles are observed with increasing concentrations of Co^{2+}. This is the evidence for lowering the crystallite size with increasing Co^{2+} concentration [15]. The average crystallite sizes estimated using the Debye Scherer formula [1,6], for as-prepared nanoparticles are shown in Table 1. As can be seen from the table, average particle sizes vary from 1.57 nm to 2.01 nm. The strain values were calculated, and it was found that there is considerable variation for pure and doped CdNS. Lower strain values indicate higher stability. Similar results are obtained in the Rietveld XRD analysis.
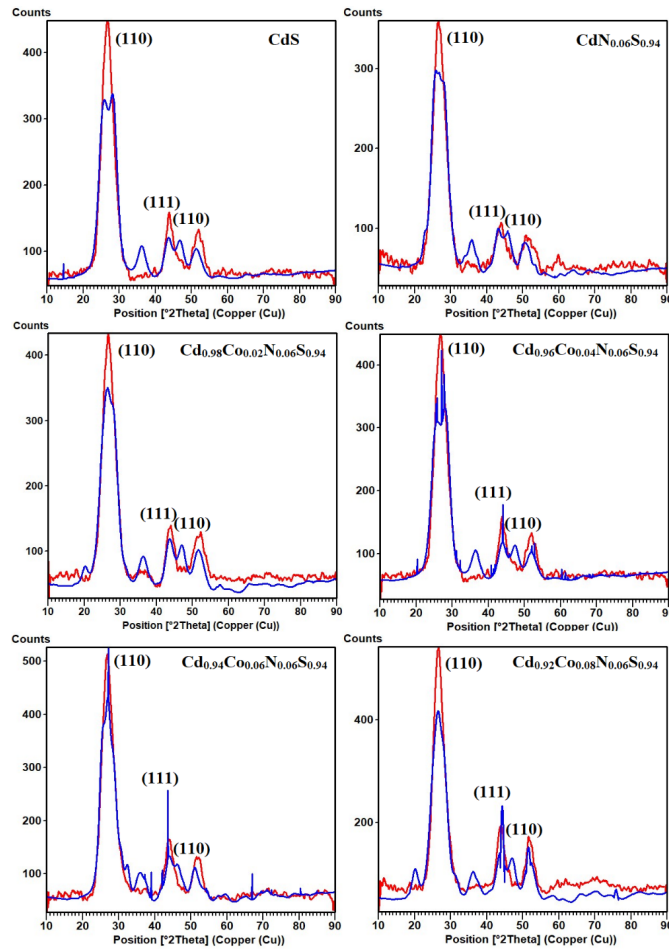
Fig 1. (a)- (e) Rietveld analysis of CdS, $Cd_{1-x}Co_xN_{0.06}S_{0.94}$ (where x=0, 0.02, 0.04, 0.06, and 0.08) nano particles

Table 1. Crystallite size and lattice strain values calculated from XRD data ofCdS,$Cd_{1-x}Co_xN_{0.06}S_{0.94}$ (where x=0, 0.02, 0.04, 0.06, and 0.08) nano particles

Compound	Crystallite Size (nm)	Lattice Strain
CdS	1.08	0.1400
$\mathbf{CdN_{0.06}S_{0.94}}$	1.57	0.0994
$\mathbf{Cd_{0.98}Co_{0.02}N_{0.06}S_{0.94}}$	1.71	0.0917
$\mathbf{Cd_{0.96}Co_{0.04}N_{0.06}S_{0.94}}$	1.75	0.0893
$\mathbf{Cd_{0.94}Co_{0.06}N_{0.06}S_{0.94}}$	1.91	0.0814
$\mathbf{Cd_{0.92}Co_{0.08}N_{0.06}S_{0.94}}$	2.01	0.0780

3.2 Elemental studies

$Cd_{1-x}Co_xN_{0.06}S_{0.94}$ (where x = 0, 0.02, 0.04, 0.06, and 0.08), CdS nanoparticles in Energy dispersive analysis of X-rays (EDAX) are shown in Figure 2. The presence of Cd and S is confirmed by very strong peaks, and the weak peaks confirm the presence of Co and N in the as-prepared nanoparticles. The ratios of elements are found to be in good agreement with their theoretically estimated stoichiometric ratios, as shown in Table 2.
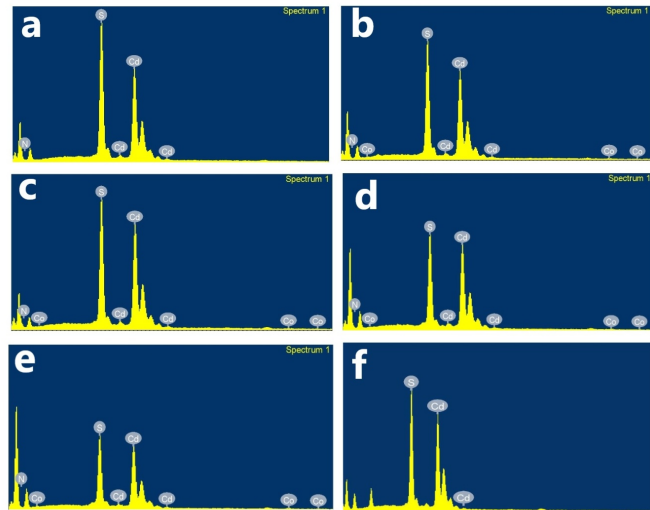
Fig 2. (a) – (e) EDAX images of $Cd_{1-x}Co_xN_{0.06}S_{0.94}$ (where x=0, 0.02, 0.04, 0.06, and 0.08), (f) CdS nanoparticles

Table 2. Percentage of atoms present in as synthesized $Cd_{1-x}Co_xN_{0.06}S_{0.94}$ nanoparticles as per EDAX

$Cd_{1-x}Co_xN_{0.06}S_{0.94}$	% of atoms present as per EDX			
	Cd	Co	N	S
x=0	49.84	0.00	6.11	44.05
x=0.02	47.02	1.98	6.12	44.88
X=0.04	45.88	3.96	6.12	44.04
x=0.06	44.09	5.87	6.11	43.83
X=0.08	41.88	8.10	5.94	44.08
CdS	49.83	–	–	50.17

3.3 Morphological studies

The high-resolution field emission scanning electron microscope (FESEM) images of $Cd_{1-x}Co_xN_{0.06}S_{0.94}$ (where x = 0, 0.02, 0.04, 0.06, and 0.08), CdS nanoparticles, are shown in Figure 3. From this, it is evident that the grain sizes gradually decrease with increasing Co^{2+} concentration, which could be due to the development of crystalline strains within the grains. An agglomeration of fine crystallites into big slabs has been observed with increasing dopant concentration.

3.4 Optical studies

3.4.1 UV-VIS spectra

The absorption band edge positions of as-prepared nanoparticles from the absorption spectra are shown in Figure 4 (a). The absorption band edges were observed from the absorption spectra of $Cd_{1-x}Co_xN_{0.06}S_{0.94}$ (where x = 0, 0.02, 0.04, 0.06, and 0.08) and are shown in Table 3 . From the Table, it is clear that the absorption band edges were initially shifted towards lower wavelengths and then shifted to higher wavelengths with increasing Co^{2+} concentration in the doped samples. A redshift has been observed in the band edge, which indicates the narrowing of the band gap[9,16].

The Tauc's plots of as-prepared nanoparticles are shown in Figure 5. From the Tauc's plot drawn between the energy hν and $(\alpha h\nu)^2$, where 'ν' is the frequency of the incident light and 'α' is the absorption coefficient of the material, bandgap values are estimated. From the Table the intrinsic CdS band gap energy (2.54 eV) is greater than the bulk CdS band gap energy (2.42 eV), which indicates the presence of a quantum confinement effect. With the inclusion of nitrogen, the bandgap value increases from 2.54 eV to 2.70 eV, then decreases to 2.39 eV with increasing cobalt concentration, which is attributed to the Burstein-Mass effect[9]. The redshift in bandgap is observed with an increase in Co^{2+} ion concentration, which could be attributed to d-d exchange interactions between the band electrons in CdS and the localized d electrons of the Co^{2+} ions[16]. The absorption band at 750nm confirms the tetrahedral phase of Co^{2+} in as-prepared nanoparticles[8]. In this way, the tailoring of the band gap
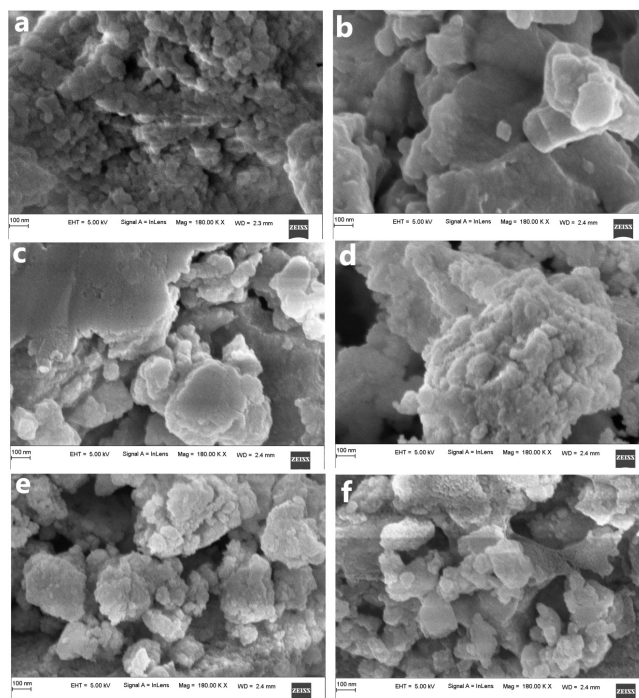
Fig 3. (a) – (f)The FESEM images of CdS, $Cd_{1-x}Co_xN_{0.06}S_{0.94}$ (where x=0, 0.02, 0.04, 0.06 and 0.08), nanoparticles
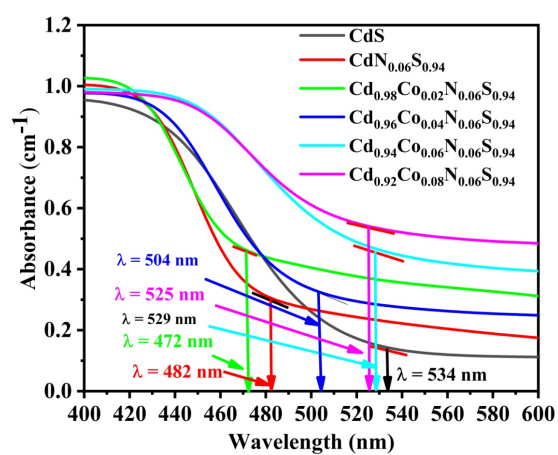
Fig 4. (a). Absorption band edge positions of CdS, $Cd_{1-x}Co_xN_{0.06}S_{0.94}$ (where x = 0, 0.02, 0.04, 0.06, and 0.08) nanoparticles
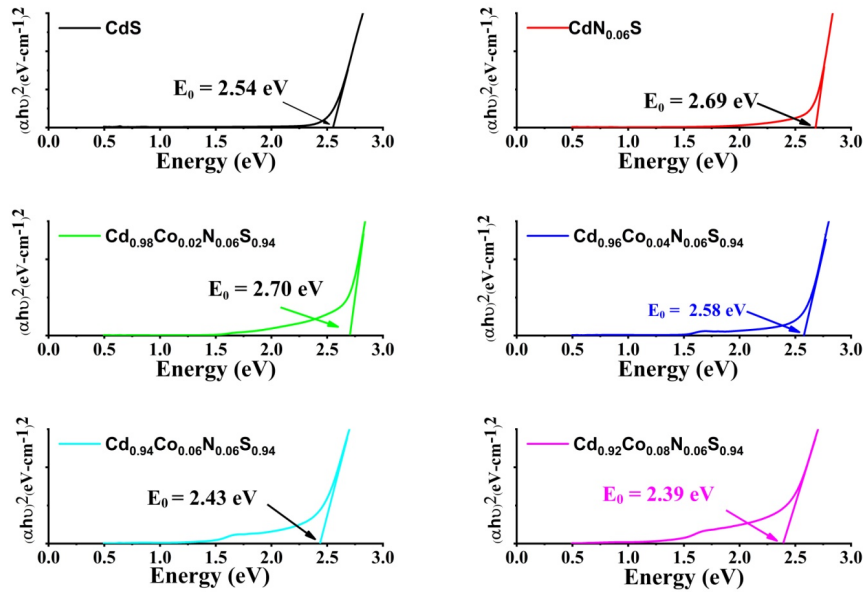
in N: CdS is possible with Co^{2+}.

Fig 5. Tauc's plots of CdS, $Cd_{1-x}Co_xN_{0.06}S_{0.94}$ (where x = 0, 0.02, 0.04, 0.06, and 0.08) nanoparticles

Table 3. Band edge position and Bandgap values of CdS, $Cd_{1-x}Co_xN_{0.06}S_{0.94}$ (where x = 0, 0.02, 0.04, 0.06, and 0.08) nano particles

Compound	Band edge position (nm)	Band gap (eV)
CdS	534	2.54
$CdN_{0.06}S_{0.94}$	482	2.69
$Cd_{0.98}Co_{0.02}N_{0.06}S_{0.94}$	472	2.70
$Cd_{0.96}Co_{0.04}N_{0.06}S_{0.94}$	504	2.58
$Cd_{0.94}Co_{0.06}N_{0.06}S_{0.94}$	529	2.43
$Cd_{0.92}Co_{0.08}N_{0.06}S_{0.94}$	525	2.39

3.5 Photoluminescence (PL) studies

Photoluminescence excitation spectra of CdS, $Cd_{1-x}Co_xN_{0.06}S_{0.94}$ (where x = 0, 0.02, 0.04, 0.06, and 0.08) monitoring the emission at 390 nm, recorded at room temperature, are shown in Figure 6. The increase or decrease in full-width at half maxima (FWHM) is the width of the peak of luminescence spectra broadened with dopant concentrations, attributed to the recombination of charge carriers trapped in the surface states[8]. The luminescence maxima observed for CdS, $Cd_{1-x}Co_xN_{0.06}S_{0.94}$ (where x = 0.02, 0.04, and 0.06) are at 512 nm, 465 nm, 488 nm, and 511 nm respectively. The clear blue shift is observed in peak positions.

The weak luminescence peak observed at 750 nm is due to near band edge emission. The blue shift in the emission peaks is attributed to the inclusion of nitrogen, with further increases in cobalt concentration, a red shift is observed. The blue emission peak is observed due to the transition of electrons from defect donor levels to valency bands, or mid gap levels.[3,8]. The IR emission peak is attributed to the presence of sulfur vacancies, i.e., F-centers[14]. There is no remarkable change in intensity up to 4% of Co^{2+} concentration, but at 6%, a greater quenching effect is observed. Co^{2+} is responsible for maintaining intensity by encouraging the radiative recombination process. The quenching effect of luminescence intensity was observed at 6% Co^{2+} concentration. It could be due to the non-radiative recombination of many excited electrons and holes at higher dopant concentrations. Dopant-induced quenching is a natural phenomenon observed in nanoparticles. A similar effect was reported in Co^{2+}-doped ZnS and CdS[2,8,17,18]. The shift in photoluminescence emission peaks is attributed to the variation of the defect's position within the bandgap.
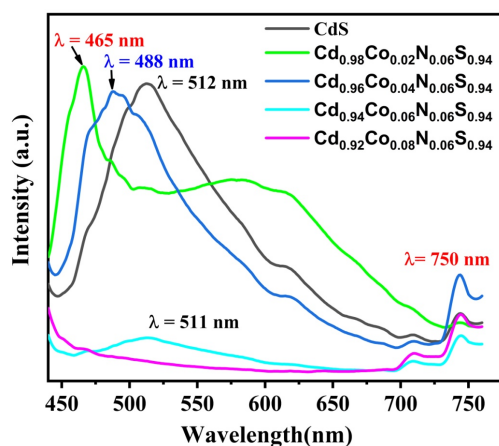
Fig 6. PL spectra of CdS, $Cd_{1-x}N_{0.06}S_{0.94}$ (Where x = 0.02, 0.04, 0.06, and 0.08) nanoparticles.

3.6 Magnetic studies

3.6.1 Electron para magnetic resonance (EPR) spectra

The EPR spectra of CdS, $Cd_{1-x}Co_xN_{0.06}S_{0.94}$ (where x = 0, 0.02, 0.04, 0.06, and 0.08) samples are shown in Figure 7. This gives information about the dopants (Co^{2+}, nitrogen) included in the prepared samples, their structure, and their magnetic behaviour. In this type, the cobalt and nitrogen ions replace the positions of Cd and S, respectively. In general, Co^{2+} (a $3d^7$ configuration) has S = ± 3/2 and I = 7/2 and exists in a high spin state with an ionic radius of 88.5 pm, possessing an eight-line hyperfine pattern. Nitrogen, with I = 1, consists of a three-line hyperfine pattern in the EPR spectra. In the present spectra, there is no hyperfine structure. This indicates that there are an increasing number of randomly distributed defects in all as-prepared nanoparticles. The intrinsic value g = 1.995, which was obtained in all previous studies, is also present in all spectra of $Cd_{1-x}Co_xN_{0.06}S_{0.94}$ (where x = 0.02, 0.04, 0.06, and 0.08), indicating the presence of nitrogen. The change in intensity is observed with an increase in the concentration of Co^{2+}. This is due to the decreasing of free ions (spin concentration) in the compound, indicating the formation of antiferromagnetic secondary compounds with dopant ions (i.e., Co_3N_2 phase) as observed in XRD analysis. This was also observed in cobalt-doped ZnO nanoparticles reported by Amalia Mesaros et al.,[19]. The peak broadening with Co^{2+} concentration indicates a shorter relaxation time and an increase in random defects in as-prepared NPs. This broadening confirms the quenching effect in the PL spectrum due to the trapping of Co^{2+} in F-centers. The zero-emission intensity magnetic fields (B_0) and their corresponding g values of as-prepared nanoparticles are determined and are shown in Table 4. These results confirm the formation of secondary compounds, which increase the stability of the nanoparticles as prepared.

The Co^{2+} ions with low spin and high spin states that exist in tetrahedral and octahedral coordination exhibit different characteristics. The octahedral field theory predicts an isotropic EPR spectrum with g = 4.3[20]. The spin-orbit coupling and excited orbital interactions for octahedral, the true g factor, vary from 2 to 9. The distorted tetrahedral geometry of high-spin Co^{2+} energy is either lower in ± 3/2 state or in ± 1/2 state. For a flattened tetrahedron, the energy is lower for ± 3/2 state, and for an elongated tetrahedron, the energy is lower for ± 1/2 state. The g factor varies from 2.2-2.4. Hence, in $Cd_{1-x}Co_xN_{0.06}S_{0.94}$ (where x = 0.04, 0.06), nanoparticles of Co^{2+} exist in a distorted tetrahedron, and in $Cd_{1-x}Co_xN_{0.06}S_{0.94}$ (where x = 0.02, 0.08), nanoparticles of Co^{2+} exist in octahedron geometry. The durability of tetrahedral coordination is higher than that of octahedral coordination[21]. The interstitial solvability of Co^{2+} ions and N^{3-} ions in tetrahedral sites of the CdS (Wurtzite structure) increases the stability of the as prepared nanoparticles. A similar effect was observed in copper- and nitrogen-doped ZnO nanoparticles by Kaur et al.,[9].

3.7 VSM Studies

In Fig. 7, M-H curves of $Cd_{1-x}Co_xN_{0.06}S_{0.94}$ (where x = 0, 0.02, 0.04, 0.06, and 0.08) nanoparticles reveal the diamagnetic property at larger values of applied field and the ferro-magnetic property in the presence of low field. It is observed that the total magnetic susceptibility consists of both diamagnetic and ferromagnetic parts, but the diamagnetic background is superimposed onto the ferromagnetic loop. After subtracting out the diamagnetic part, the ferromagnetic response at different concentrations

Table 4. B_0 and g values calculated from EPR spectra of $Cd_{1-x}Co_xN_{0.06}S_{0.94}$ (where x=0, 0.02, 0.04, 0.06, and 0.08) nanoparticles

Sample↓↓ Property→	B_0(mT)	$B_{||}$ (mT)	$B_\perp$ (mT)	g	$g_\perp$	$g_{||}$
x =0	306	288	350	2.20	2.57	1.96
x =0.02	195	214	178	3.39	3.69	3.20
x =0.04	337	336	338	2.00	2.01	1.99
x =0.06	337	336	338	2.00	2.01	1.99
x =0.08	308	289	349	2.23	2.91	1.91
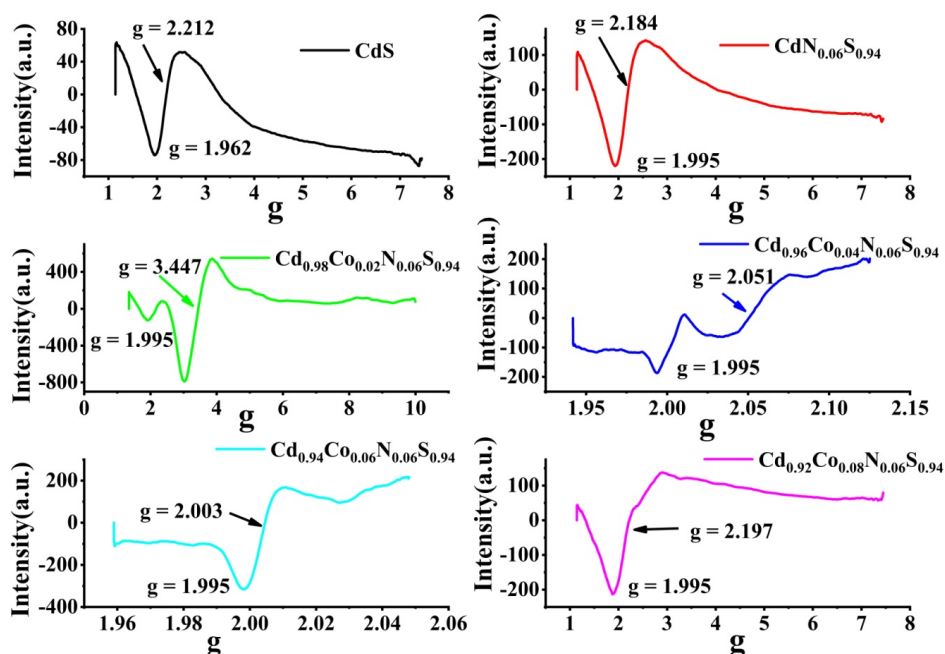
Fig 7. EPR spectra of CdS, $Cd_{1-x}Co_xN_{0.06}S_{0.94}$ (where x=0, 0.02, 0.04, 0.06, and 0.08) nanoparticles

of Co^{2+} is plotted in the inset of Figure 8. The open curves at room temperature are due to an increase in Co^{2+} concentration, which indicates the room temperature ferromagnetic (RTFM) nature of the $Cd_{1-x}Co_xN_{0.06}S_{0.94}$ (where x = 0, 0.02, 0.04, 0.06, and 0.08) nanoparticles. The ferromagnetic property rises due to certain local defects in the crystal, interactions between the secondary compounds formed by doping elements, and the nature of the carrier medium. Giribabu et al., reported that the RTFM is the cobalt ion's intrinsic property in CdS[8]. No reports are available on nitrogen-cobalt-co-doped CdS. In the present study, the PL studies showed the formation of certain defects at different positions by shifting peak positions and broadening peaks. The XRD studies show the presence of Co_3N_2. The EPR studies confirmed the presence of antiferromagnetic secondary compounds in the as-prepared samples. Hence, the RTFM values at low fields are attributed to the local defects, the interaction between the secondary compounds, and the Co^{+2} metallic ions present in the as-prepared nanoparticles.

With an increase in the applied magnetic field and concentration of the metallic ions Co^{2+} the samples first turned paramagnetic and then dia. According to the theory of bound magnetic polaron (BPM)[22], in DMS, the ferromagnetism is a long-range carrier-mediated component, and the anti-ferromagnetism is a short-range direct exchange interaction. At lower concentrations of Co^{2+}, the range is larger, and antiferromagnetic interactions are negligible. At higher concentrations, the stretches in the EPR signal indicate a shorter life time, which demotes the ferromagnetism. As the applied field increases, the antiferromagnetic interactions suppress the ferromagnetism. Ferromagnetic and antiferromagnetic coupling attribute to the novel magnetic behaviour of the as-prepared samples. Surya et al., reported similar property in N doped Cr: CdS[23]. In this way, tailoring of inherent magnetism is possible with Co^{2+}, which has potential for spintronic devices.
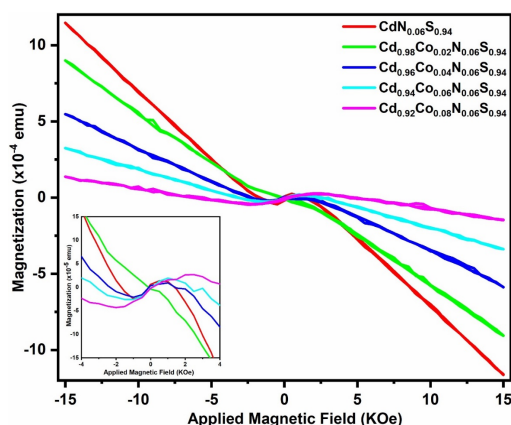
Fig 8. VSM spectra of $Cd_{1-x}Co_xN_{0.06}S_{0.94}$ (where x=0, 0.02, 0.04, 0.06, and 0.08) nanoparticles

4 Conclusion

Using the chemical co-precipitate method, cobalt and nitrogen-co-doped CdS nanoparticles are synthesized successfully with less than 2nm size. The XRD and EPR studies confirmed that the particles exist in a composite phase, which leads to an increase in stability. The X'pert high score analysis and EPR studies confirmed the inclusion of cobalt and nitrogen in the tetrahedral phase, which is the most stable phase. UV-VIS studies showed a clear Burstein mass effect with an increase in Co^{2+} concentration and tuning of band gap values with dopant concentrations between 2.3 and 2.7 eV. PL studies confirmed dopant-induced quenching at 6% of Co^{2+} concentration due to the non-radiative recombination of many excited electrons and holes at higher dopant concentrations. VSM studies showed that the nanoparticles exhibit ferromagnetic properties at low fields. The magnetic phase transition from ferro to dia through paramagnetism is observed with an applied field and a concentration of Co^{2+}. This tuning of band gap values and magnetic properties with dopant concentrations has potential for optomagnetic and spintronic devices.

References

1) Muruganandam S, Parivathini K, Murugadoss G. Effect of co-doped (Ni2+:Co2+) in CdS nanoparticles: investigation on structural and magnetic properties. *Applied Physics A*. 2021;127(6):1–9. Available from: https://doi.org/10.1007/s00339-021-04555-0.

2) Patel NH, Deshpande MP, Chaki SH. Influence of Co-doping on the optical and magnetic properties of CdS nanoparticles. *Journal of Materials Science: Materials in Electronics*. 2018;29(13):11394–11403. Available from: https://doi.org/10.1007/s10854-018-9230-x.

3) Maddi L, Vinukonda K, Gurugubelli TR, Koutavarapu R. One-Step Situ Hydrothermal Fabrication of Cobalt-Doped ZnO/CdS Nanosheets for Optoelectronic Applications. *Electronics*. 2023;12. Available from: https://doi.org/10.3390/electronics12051245.

4) Nayak S, Kumar P. Review on structure, optical and magnetic properties of cobalt doped ZnO nanoparticles. *Materials Today: Proceedings*. 2023. Available from: https://doi.org/10.1016/j.matpr.2023.01.318.

5) Jeevanantham N, Balasundaram ON. High-performance visible light photocatalytic activity of cobalt (Co) doped CdS nanoparticles by wet chemical route. *Journal of the Iranian Chemical Society*. 2019;16(2):243–251. Available from: https://doi.org/10.1007/s13738-018-1499-4.

6) Heiba ZK, Mohamed MB, Plaisier JR, El-Naggar AM, Albassam AA. Influence of (Mn or Co)-doping on structural, magnetic and electronic properties of nano Zn0.75Cd0.25S. *Chinese Journal of Physics*. 2020;67:414–427. Available from: https://doi.org/10.1016/j.cjph.2020.04.010.

7) Poornaprakash B, Subramanyam K, Cheruku R, Kim YL, Reddy MSP, Reddy VRM. Mn and Al co-doped CdS:Cr nanoparticles for spintronic applications. *Materials Science in Semiconductor Processing*. 2021;134:106055. Available from: https://doi.org/10.1016/j.mssp.2021.106055.

8) Giribabu G, Murali G, Reddy DA, Liu C, Vijayalakshmi RP. Structural, optical and magnetic properties of Co doped CdS nanoparticles. *Journal of Alloys and Compounds*. 2013;581:363–368. Available from: https://doi.org/10.1016/j.jallcom.2013.07.082.

9) Kaur M, Kumar V, Singh J, Datt J, Sharma R. Effect of Cu-N co-doping on the dielectric properties of ZnO nanoparticles. *Materials Technology*. 2022;37(13):2644–2658. Available from: https://doi.org/10.1080/10667857.2022.2055909.

10) Yan X, Tu Y, Yuan H, Xia Y, Jiang Y, Zhu S, et al. Experimental and theoretical insights into cobalt nanoparticles encapsulated in N- and S-codoped carbon as advanced bifunctional electrocatalyst for rechargeable zinc-air batteries. *Advanced Composites and Hybrid Materials*. 2023;6(2). Available from: https://doi.org/10.1016/j.apmate.2021.12.003.

11) Zhang X, Yan F, Zhang S, Yuan H, Zhu C, Zhang X, et al. Hollow N-Doped Carbon Polyhedron Containing CoNi Alloy Nanoparticles Embedded within Few-Layer N-Doped Graphene as High-Performance Electromagnetic Wave Absorbing Material. *ACS Applied Materials & Interfaces*. 2018;10(29):24920–24929. Available from: https://doi.org/10.1021/acsami.8b07107.

12) Shi W, Guo F, Li M, Shi Y, Tang Y. N-doped carbon dots/CdS hybrid photocatalyst that responds to visible/near-infrared light irradiation for enhanced photocatalytic hydrogen production. *Separation and Purification Technology*. 2019;212:142–149. Available from: https://doi.org/10.1016/j.seppur.2018.11.028.

13) Jia L, Wang DHH, Huang YXX, Xu AWW, Yu HQQ. Highly Durable N-Doped Graphene/CdS Nanocomposites with Enhanced Photocatalytic Hydrogen Evolution from Water under Visible Light Irradiation. *The Journal of Physical Chemistry C*. 2011;115(23):11466–11473. Available from: https://doi.org/10.1021/jp2023617.

14) Popov IS, Kozhevnikova NS, Melkozerova MA, Vorokh AS, Enyashin AN. Nitrogen-doped ZnS nanoparticles: Soft-chemical synthesis, EPR statement and quantum-chemical characterization. *Materials Chemistry and Physics*. 2018;215:176–182. Available from: https://doi.org/10.1016/j.matchemphys.2018.04.115.

15) Misra KP, Jain S, Agarwala A, Halder N, Chattopadhyay S. Effective Mass Model Supported Band Gap Variation in Cobalt-Doped ZnO Nanoparticles Obtained by Co-Precipitation. *Semiconductors*. 2020;54(3):311–316. Available from: https://doi.org/10.1134/S1063782620030136.

16) Ibraheem F, Mahdy MA, Mahmoud EA, Ortega JE, Rogero C, Mahdy IA, et al. Tuning Paramagnetic effect of Co-Doped CdS diluted magnetic semiconductor quantum dots. *Journal of Alloys and Compounds*. 2020;834:155196. Available from: https://doi.org/10.1016/j.jallcom.2020.155196.

17) Popov ID, Kuznetsova YV, Rempel SV, Rempel AA. Tuning of optical properties of CdS nanoparticles synthesized in a glass matrix. *Journal of Nanoparticle Research*. 2018;20(3). Available from: https://doi.org/10.1007/s11051-018-4171-0.

18) Patel NH, Deshpande MP, Chaki SH. Influence of Co-doping on the optical and magnetic properties of CdS nanoparticles. *J Mater Sci: Mater Electron*. 2018;29:11394–11403. Available from: https://doi.org/10.1007/s10854-018-9230-x.

19) Mesaros A, Ghitulica CD, Popa M, Mereu R, Popa A, Petrisor T, et al. Synthesis, structural and morphological characteristics, magnetic and optical properties of Co doped ZnO nanoparticles. *Ceramics International*. 2014;40(2):2835–2846. Available from: https://doi.org/10.1016/j.ceramint.2013.10.030.

20) Kumar S, Sharma JK. Stable phase CdS nanoparticles for optoelectronics: a study on surface morphology, structural and optical characterization. *Materials Science-Poland*. 2016;34(2):368–373. Available from: https://doi.org/10.1515/msp-2016-0033.

21) Muruganandam S, Anbalagan G, Murugadoss G. Optical, electrochemical and thermal properties of Co2+-doped CdS nanoparticles using polyvinylpyrrolidone. *Applied Nanoscience*. 2015;5(2):245–253. Available from: https://doi.org/10.1007/s13204-014-0313-6.

22) Kaminski A, Sarma SD. Polaron Percolation in Diluted Magnetic Semiconductors. *Physical Review Letters*. 2002;88(24):4–4. Available from: https://doi.org/10.1103/PhysRevLett.88.247202.

23) Reddy MSS, Sai C, Vandana YB, Kumar. Room Temperature Ferromagnetism and Enhanced Band Gap Values in N Co-doped Cr: CdS Nanoparticles for Spintronic Applications. *Journal of Superconductivity and Novel Magnetism* . 2023;36(4):1243–1248. Available from: https://doi.org/10.1007/s10948-023-06565-w.